The Journal of Chemical Physics

Tetrel, chalcogen, and CH···O hydrogen bonds in complexes pairing carbonyl-containing molecules with 1, 2, and 3 molecules of CO_2

Cite as: J. Chem. Phys. **142**, 034307 (2015); https://doi.org/10.1063/1.4905899
Submitted: 29 November 2014 . Accepted: 02 January 2015 . Published Online: 20 January 2015

Luis M. Azofra, and Steve Scheiner

Tetrel, chalcogen, and CH··O hydrogen bonds in complexes pairing carbonyl-containing molecules with 1, 2, and 3 molecules of CO_2

Luis M. Azofra[1] and Steve Scheiner[2,a)]
[1]*Instituto de Química Médica, CSIC, Juan de la Cierva, 3, E-28006 Madrid, Spain*
[2]*Department of Chemistry and Biochemistry, Utah State University, Logan, Utah 84322-0300, USA*

(Received 29 November 2014; accepted 2 January 2015; published online 20 January 2015)

The complexes formed by H_2CO, CH_3CHO, and $(CH_3)_2CO$ with 1, 2, and 3 molecules of CO_2 are studied by *ab initio* calculations. Three different types of heterodimers are observed, most containing a tetrel bond to the C atom of CO_2, and some supplemented by a CH··O H-bond. One type of heterodimer is stabilized by an anti-parallel arrangement of the C=O bonds of the two molecules. The binding energies are enhanced by methyl substitution on the carbonyl, and vary between 2.4 and 3.5 kcal/mol. Natural bond orbital analysis identifies a prime source of interaction as charge transfer into the π*(CO) antibonding orbital. Heterotrimers and tetramers carry over many of the geometrical and bonding features of the binary complexes, but also introduce O··O chalcogen bonds. These larger complexes exhibit only small amounts of cooperativity. [http://dx.doi.org/10.1063/1.4905899]

INTRODUCTION

Carbon dioxide (CO_2) is a fundamental molecule involved in many natural and industrial processes. It is an essential part of the carbon cycle and a main product of cellular respiration.[1] CO_2 is also produced in massive amounts from the carbon combustion that contributes so heavily to the greenhouse effect.[2] Another important feature of CO_2 is its supercritical character[3] at 304.25 K and 7.39 MPa. It has been the subject of research involving so-called green solvents, i.e., solvents that have minimal environmental impact (cost, safety, and health issues).[4]

Experimental work has been aimed toward greater understanding of the behavior of supercritical CO_2 (sc-CO_2) as solvent for organic compounds.[5–10] CO_2 has also been the subject of numerous computational studies.[11–16] Other efforts have added to understanding the interactions of CO_2 with various solutes, especially those containing carbonyl functional groups or aromatic systems and other heteroatoms as nitrogen, sulfur, or halogens in their compositions.[17–28] These works have added to our understanding by providing a clear definition of the conformational landscape in systems in which CO_2 acts as both electron acceptor and donor in noncovalent complexes with different solutes and in the presence of a variety of heteroatoms in their compositions, which offer many peculiarities in their structures.

The recent development of the concept of chalcogen bond[29–48] leads naturally to the need to explore the importance of such bonds that involve CO_2. Also relevant are the recent findings that the C atom can participate in fairly strong noncovalent bonds, commonly referred to as tetrel bonds.[49–51] It is thus important to investigate the strength of interactions between CO_2 and carbonyl-containing molecules, as well as the underlying nature of these bonds. As there is a strong interest in CO_2 as a solvent, it is imperative to consider aggregates in which a solute molecule is surrounded by a number of CO_2 molecules, an area which remains largely unexplored at present.

This work addresses these issues by first allowing a molecule of CO_2 to interact with the carbonyl containing H_2CO, CH_3CHO, and $(CH_3)_2CO$ systems. Calculation of the full potential energy surface (PES) of each heterodimer reveals all minima, and careful analysis then provides insights into the fundamental nature of the bonding. Expansion of the system by addition of more CO_2 molecules shows how the geometry and bonding in the heterodimer is affected by placement of the solute in an environment more akin to solvation, and particularly the magnitude of cooperative effects.

Some earlier work in this area[52–55] can act as a guide. Prior calculations studied some of the heterodimers examined here, but were limited in a number of respects. In the first place, each paper considered a different system and with a different level of theory, sometimes with a basis set as small as 6-31G, so comparisons are difficult. Nor did any of the earlier work include a thorough search of the potential energy surface of any of these heterodimers, so there are certain minima that were missed. Unlike the multipronged analysis of the wave function carried out below, there was little attempt to understand the source of the binding in these systems. And none of the earlier work considered complexes larger than the 1:1 dimer level, so obtained no information relevant to aggregates and cooperativity, important aspects of clustering.

COMPUTATIONAL DETAILS

The geometry and properties of the $(CO_2)_n$:H_2CO, $(CO_2)_n$:CH_3CHO, and $(CO_2)_n$:$(CH_3)_2CO$ complexes ($n = 1$, 2, 3) were studied through the use of the second-order Møller-Plesset perturbation theory (MP2).[56] Dunning's aug-cc-pVTZ[57] basis set was used for the optimization of the 1:1 and

a)Author to whom correspondence should be addressed. Electronic mail: steve.scheiner@usu.edu. Fax: (+1) 435-797-3390.

2:1 CO_2:solute heterodimers and trimers, while optimization was carried out with the smaller aug-cc-pVDZ basis for 3:1 CO_2:solute heterotetramers, due to the size of these systems. To ensure comparable values between heterotetramers and less solvated systems, single-point MP2/aug-cc-pVTZ calculations were performed. Frequency calculations confirmed the nature of the stationary points as true minima and enabled the computation of zero point energy (ZPE). Binding energies, E_b, were computed as the difference in energy between the complex on one hand and the sum of the energies of the optimized monomers on the other. Also, the counterpoise procedure was used to correct the basis set superposition error (BSSE) in the heterodimers.[58] All calculations were carried out via the GAUSSIAN09 (revision D.01)[59] and MOLPRO[60] programs.

The many-body procedure[61,62] was applied to ternary [Eq. (1)] and quaternary [Eq. (2)] complexes whereby the binding energy can be expressed as

$$E_b(\text{ternary}) = E_r + \Sigma\Delta^2 E + \Delta^3 E, \quad (1)$$

$$E_b(\text{quaternary}) = E_r + \Sigma\Delta^2 E + \Sigma\Delta^3 E + \Delta^4 E, \quad (2)$$

where $\Delta^n E$ is the n^{th} complex term (2 = for binary, 3 = for ternary, and 4 = for quaternary complexes), and the largest value of n represents the total cooperativity in the full complex. E_r represents the energy of deformation of each monomer in forming the complex.

Natural bond orbital (NBO)[63] theory with the ωB97XD[64] functional was applied to help analyze the interactions, using the NBO6.0[65] program. The presence of charge transfers between natural orbitals of different fragments supports the presence of attractive bonding interactions. AIM analysis[66] added complementary information about the presence and strength of intermolecular bonds; these calculations were carried out with the AIMAll program.[67] Another methodology used on occasion for analysis of noncovalent interactions is the NCI index, which visualizes three-dimensional regions as either attractive or repulsive forces; the NCI index has been calculated via the NCIPLOT program.[68] Additionally, the molecular electrostatic potential (MEP)[69] on the 0.001 a.u. electron density isosurface of each monomer was evaluated via the WFA-SAS program.[70]

Finally, DFT-SAPT calculations were carried out at the PBE0[71]/aug-cc-pVTZ computational level. The interaction energy using this methodology, $E^{\text{DFT-SAPT}}$, is obtained as a sum of five terms [Eq. (3)]: electrostatic (E_{ele}), exchange (E_{exc}), induction (E_{ind}), dispersion (E_{dis}), and higher-order term contributions (δ_{HF}).[72] Asymptotic corrections were included using the experimental ionization potential for the CO_2 (Ref. 73) and CH_3CHO (Ref. 74) molecules. All these calculations were performed using the MOLPRO program.[60]

$$E^{\text{DFT-SAPT}} = E_{ele} + E_{exc} + E_{ind} + E_{dis} + \delta_{HF}. \quad (3)$$

RESULTS AND DISCUSSION

Properties of monomers

In 2012, Altarsha *et al.*[18] and subsequently, in 2013, Azofra *et al.*[20] rationalized in depth the nature of the interactions between CO_2 and simpler carbonyl compounds, as aldehydes, ketones, amides, and carbamides, in terms of Lewis acid and base concepts. As indicated in Scheme 1, three kinds of structures were proposed. Type I is characterized by the presence of a C··O CO_2/solute tetrel interaction and an OCO··H hydrogen bond (HB); subtypes a and b indicate, respectively, whether the bridging H is located on the carbonyl C or a methyl group. Type II eschews the CH··O HB, instead placing the C of CO_2 directly along the C═O axis. An O atom of CO_2 engages in a C··O tetrel bond with the carbonyl C in type III structures.

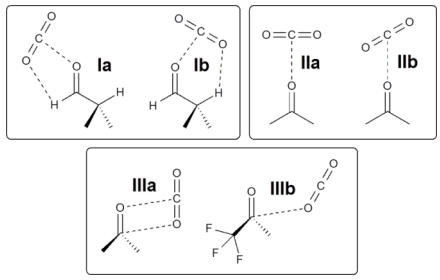

SCHEME 1. CO_2:solute heterodimer structures based on Lewis acid and base concepts.[18,20]

Potential geometries of binary complexes can also be envisioned on the basis of purely Coulombic factors. The MEP of each monomer is illustrated in Fig. 1, where red and blue regions indicate negative and positive regions, respectively. The MEP of CO_2 is negative at the O ends of the C═O bonds, and positive otherwise, especially on an equatorial belt surrounding the C atom. The MEP minima on the 0.001 a.u. electron density isosurface are rather small in magnitude, with $V_{s,min} = -10.7$ kcal/mol, as compared to a much larger positive value of 26.1 kcal/mol on the molecule's equator. The potentials surrounding the carbonyl molecules are largely positive, with lobes along the extension of the C—H bonds. These lobes correspond to $V_{s,max} = 21.8$ kcal/mol in H_2CO and 14.5 and 11.6 kcal/mol for the H atoms of CH_3CHO and $(CH_3)_2CO$, respectively. A region of negative potential surrounds the O atom in each solute. As the number of methyl groups grows, so does the value of $V_{s,min}$, varying as −29.0, −32.8, and −35.1 kcal/mol for H_2CO, CH_3CHO, and

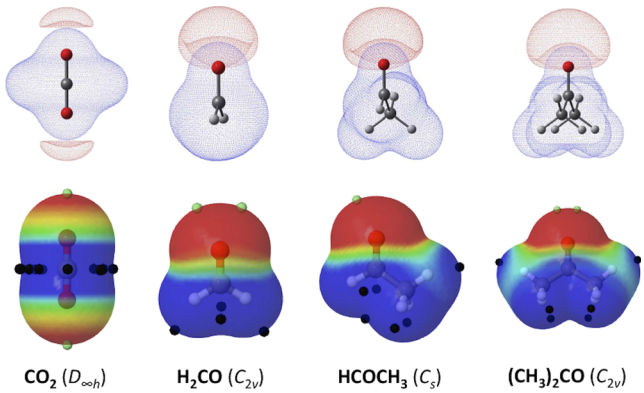

FIG. 1. MEP at the MP2/aug-cc-pVTZ computational level for the CO_2, H_2CO, $HCOCH_3$, and $(CH_3)_2CO$ monomers. Red and blue regions indicate negative and positive potentials, respectively. (Top) The ±0.015 a.u. (CO_2) and ±0.035 a.u. (others) isocontours. (Bottom) MEP on the 0.001 a.u. electron density isosurface, where light green and black spheres represent minima (lone pairs) and maxima (π- or σ-holes), respectively.

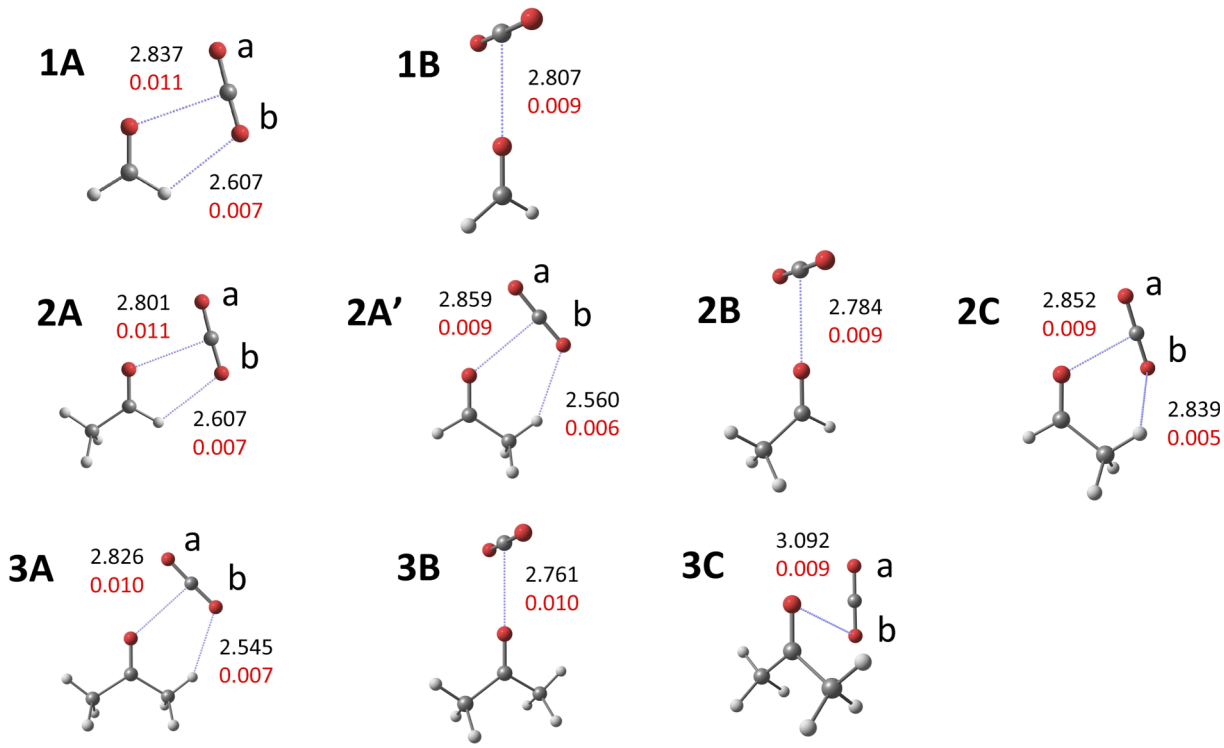

FIG. 2. Structures of minima on the potential energy surfaces of indicated heterodimers at the MP2/aug-cc-pVTZ computational level. Broken lines are shown between atoms deemed by AIM to be connected by a bond critical point. Density at this point indicated in red (a.u.) and interatomic distance in black (Å).

$(CH_3)_2CO$, respectively. Finally, H_2CO and CH_3CHO contain π-holes above the C(sp^2) atom, with $V_{s,max}$ values of 25.5 and 21.1 kcal/mol. If it were based solely on electrostatic considerations, then, one might expect the strength of the interaction between CO_2 and each carbonyl molecule to grow as H atoms are progressively replaced by methyl groups.

1:1 CO_2:solute complexes

There are three types of structures identified as minima in the PES of each heterodimer. These geometries are illustrated in Fig. 2 in which atoms deemed to be connected by a bond critical point (BCP) by AIM are connected by a broken line, with the value of the density at this point indicated in red. The A geometries on the left side of Fig. 2, generally the most stable, contain two noncovalent bonds. The stronger of these two bonds is shown by NBO analysis to involve electron donation from the carbonyl O lone pairs to π* antibonding orbitals of CO_2, specifically to the C═O_a bond. (Note that AIM places the bond between the carbonyl O and the CO_2 C atom.) Also present is a CH··O HB to the other O_b atom of CO_2. The binding energies of these structures reported in the first column of Table I are in the range between 3.1 and 3.4 kcal/mol (2.7 and 2.9 kcal/mol following BSSE correction), and rise in the order $H_2CO < CH_3CHO < (CH_3)_2CO$. Although the aldehydic CH of CH_3CHO is nominally a more potent donor than the methyl H, geometric distortions within the CH··O HB in 2A weaken this interaction in comparison to 2A′. The latter displays a shorter CH··O distance, and perhaps more importantly a more linear arrangement, with θ(CH··O) = 144° in 2A′ as compared to 112° in 2A. This superior alignment is also reflected in the NBO E(2) for $O_{lp} \rightarrow \sigma^*(CH)$ which is 0.74 *vs.* 0.31 kcal/mol for 2A′ and 2A, respectively. On the other hand, the Laplacian of the electron

TABLE I. Thermodynamic quantities for formation of indicated heterodimers at MP2/aug-cc-pVTZ computational level and 298 K. All quantities in kcal/mol, except ΔS in cal mol^{-1} K^{-1}. Also, break temperature for spontaneous/non-spontaneous Gibbs free energy in K.

Complex	Symmetry	ΔE[a]	ΔE + ZPE	ΔH	ΔS	ΔG	$T_{G=0}$
1A	C_s	−3.06 (−2.65)	−2.27	−2.06	−20.12	3.93	102.4
2A	C_s	−3.35 (−2.89)	−2.74	−2.37	−21.78	4.13	108.8
2A′	C_s	−3.16 (−2.67)	−2.64	−2.20	−19.54	3.62	112.6
3A	C_s	−3.44 (−2.89)	−2.89	−2.48	−22.49	4.23	110.3
1B	C_{2v}	−2.39 (−2.09)	−1.90	−1.44	−14.53	2.90	99.1
2B	C_{2v}	−2.69 (−2.34)	−2.30	−1.74	−14.18	2.48	122.7
3B	C_{2v}	−2.98 (−2.57)	−2.63	−2.04	−10.25	1.02	199.0
2C	C_1	−3.09 (−2.60)	−3.63	−2.16	−19.03	3.51	113.5
3C	C_s	−3.53 (−2.86)	−3.07	−2.62	−22.29	4.03	117.5

[a]In parentheses, energies corrected with the BSSE via the counterpoise procedure.

density at the BCP is slightly smaller, 0.026 a.u. in 2A′ as compared to 0.031 in 2A. The energetic preference of 2A over 2A′ must therefore be attributed to a stronger O··C tetrel bond, with R(C··O) shorter in 2A by 0.06 Å.

The calculations indicate that ΔG is positive for all binary complexes at room temperature, with values between 1 and 4 kcal/mol. Although the equilibrium concentrations of these heterodimers will be small at this temperature, the negative values of ΔH argue that these concentrations will rise as the temperature declines. Taking 2A as an example, ΔG is equal to +4.13 kcal/mol at T = 298 K, but becomes negative for temperatures below 109 K. In the case of 3B, the transition point to negative ΔG occurs at 200 K.

The growing strength of the interaction arising from the addition of methyl groups is likely connected with the progressively more negative potential surrounding the carbonyl O atom. And this same trend is consistent with the notion that methyl groups are electron-releasing in nature. With regard to the C··O bond, the R(C··O) distance is shortest (2.801 Å) for CH_3CHO 2A, which also exhibits the largest NBO charge transfer stabilization energies, E(2) $O_{lp} \rightarrow \pi^*(CO_a)$ of 2.3 kcal/mol, as displayed in Table II. The R(CH··O_a) HB lengths are roughly 2.6 Å, distorted from linearity, and E(2) $O_{lp} \rightarrow \sigma^*(CH)$ is in the 0.3-0.7 kcal/mol range, making this CH··O HB considerably weaker than C··O. Note also that the bonds in these cyclic complexes of type A would be expected to reinforce one another in that each molecule serves as both electron donor and acceptor.

The second B type of geometry places the CO_2 C atom directly along the C═O axis, forgoing any sort of CH··O HB. The OCO molecule lies perpendicular to the aldehyde plane. The resulting R(C··O) distances are slightly shorter than in the A structures, but E(2) $O_{lp} \rightarrow \pi^*(CO)$ smaller, in the 1.0-1.4 kcal/mol range. The values of ρ at the BCP are also slightly smaller than in the A complexes. Like the A binary complexes, the binding strength grows as methyl groups are added to the aldehyde. The B heterodimers are roughly 0.5 kcal/mol more weakly bound than the A geometries.

A third sort of minimum occurs on the PES for both CH_3CHO and $(CH_3)_2CO$. 3C is in fact the global minimum on this surface, bound more strongly than 3A by 0.1 kcal/mol, but indistinguishable energetically following counterpoise correction. Like the A structures, the C heterodimers contain a C··O tetrel bond, but any CH··O HB is either weakened by its length (2C) or nonexistent altogether (3C). They are arranged instead so that one of the two C═O bonds of CO_2 lies directly above the C═O of the aldehyde in an anti-parallel geometry. This arrangement facilitates transfer not only from the aldehyde O lone pairs to π*(CO) but also from the π(CO) orbitals, as indicated in Table II. NBO thus differs to some extent with AIM which portrays a chalcogen O··O_b bond for the 3C heterodimer. In the case of 2C, this supplementary transfer goes in the same direction, from aldehyde to CO_2, and amounts to 0.33 kcal/mol. In contrast, the transfer of 0.74 kcal/mol is in the opposite direction in 3C from π(CO) of CO_2 to π*(CO) of the aldehyde. The stability of this 3C structure may reside then in the fact that each molecule acts as both donor and acceptor. Indeed, the highest binding energy of all heterodimers considered here is that of 3C attesting to the strength of this sort of C··O binding. It is curious to note that the AIM procedure predicts a HB between the O atom of CO_2 and one of the H atoms of the methyl group in 2C. In contrast, there is only a meager 0.05 kcal/mol reported by NBO for the associated $O_{lp} \rightarrow \sigma^*(CH)$ charge transfer E(2).

TABLE II. E(2) NBO values (kcal/mol) at ωB97XD/aug-cc-pVTZ computational level for indicated transfers in heterodimers.

Complex	$O_{lp} \rightarrow \pi^*(CO_a)$	$O_{lp} \rightarrow \sigma^*(CH)$	$\pi(CO) \rightarrow \pi^*(CO)$
1A	2.06	0.32	···
2A	2.30	0.31	···
2A′	1.59	0.74	···
3A	1.84	0.74	···
1B	1.07	···	···
2B	1.13	···	···
3B	1.37	···	···
2C	1.13	···	0.33[a]
3C	1.41	···	0.74[b]

[a]From CO_2 to C=O.
[b]From C=O to CO_2.

The bond length changes that accompany the formation of each binary complex offer an alternate perspective on the nature of the bonding. The aldehydic C═O bond elongates in A complexes by 1.5-1.8 mÅ, and slightly less (1.2 mÅ) in C structures. Within CO_2, the C═O_a bond which is the recipient of the charge transfer from the carbonyl lone pairs is shortened by 2 mÅ in the A and C structures, while the other C═O_b bond is elongated by a comparable amount. The bond lengths are affected to a lesser degree in the B geometries, with small (<0.5 mÅ) elongations of the carbonyl C═O and contractions of the C═O bonds in CO_2.

For all heterodimer types, inclusion of zero-point vibrational energy reduces the binding energy by some 0.4-0.8 kcal/mol, leading to corrected values between −1.9 and −3.1 kcal/mol. When all corrections are added, ΔH is about 1.0 kcal/mol less negative than ΔE, as may be noted in Table I. Following incorporation of the loss of entropy upon dimerization, the values of ΔG are all positive at 298 K.

The heterodimers of CO_2 with several carbonyl molecules were partially studied earlier[52–55] and subsequently by Altarsha *et al.*,[18] who did not carry out thorough searches of the potentials, but instead optimized only selected geometries. Rather than our aug-cc-pVTZ basis set, Altarsha *et al.*[18] optimized structures with the smaller aug-cc-pVDZ. They only noted one minimum on the H_2CO surface which corresponds to our 1A geometry, with slightly longer interatomic distances. They identified only two (of our four) minima for CH_3CHO, corresponding to our 2A and 2A′, and only found two of our three minima for CH_3COCH_3, 3A and 3C. The smaller basis of Altarsha *et al.* yielded somewhat different values of NBO E(2) at the SCF level, but the results were qualitatively similar to our data with aug-cc-pVTZ which also included correlation via ωB97XD. However, they unfortunately did not provide any AIM data or bond length changes with which our values might be compared. Raman spectroscopic data[75] are consistent with structure 2A for the complex of CO_2 with acetaldehyde, although not fully conclusive.

The NCI index evaluated for the CO_2:CH_3CHO heterodimers (the system in which all three of A, B, and

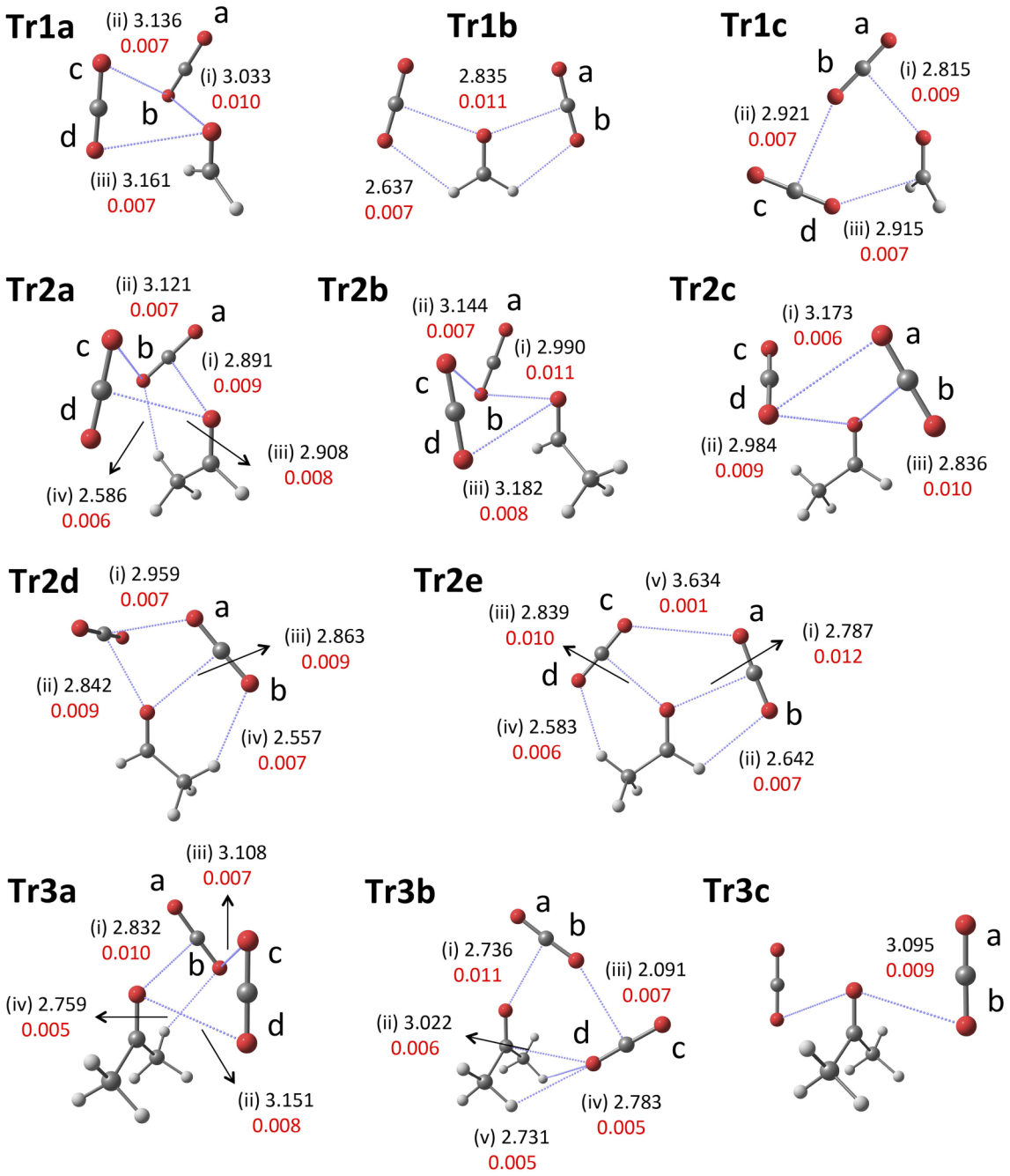

FIG. 3. Structures of minima on the potential energy surfaces of indicated heterotrimers at the MP2/aug-cc-pVTZ computational level. Broken lines are shown between atoms deemed by AIM to be connected by a bond critical point. Density at this point indicated in red (a.u.) and interatomic distance in black (Å).

C type 1:1 complexes were found) supports the AIM and NBO results. The C··O tetrel bonds of all four of these heterodimers are confirmed by the green regions between the two pertinent atoms via indexes in the green contour with $\rho \approx 0$ and $\lambda_H \approx 0$. (See Fig. S1 of the supplementary material.[84]) The same is true for the purported CH··O H-bonds in 2A, 2A′, and 2C. NCI thus agrees with the AIM finding of such a H-bond in 2C.

Finally, DFT-SAPT analysis at the PBE0/aug-cc-pVTZ computational level, in Table S1 of the supplementary material,[84] reveals that the term of greatest magnitude is the repulsive exchange energy, E_{exc}. The electrostatic component E_{ele} is the largest attractive term, followed by the dispersion, E_{dis}; induction is considerably smaller.

2:1 and 3:1 CO_2:solute complexes

A second CO_2 molecule was added to each heterodimer, and the PES of the resulting 2:1 complex was explored to identify all minima. A dual search procedure was followed. First, the second CO_2 molecule was incorporated into the heterodimer minima. Additional starting points were generated from fresh initial structures by random selection[76] in order to ensure proper consideration of geometries not related to these heterodimers.

The resulting 2:1 CO_2:solute heterotrimer structures, optimized again at the MP2/aug-cc-pVTZ level, are displayed in Fig. 3. As for the heterodimers, each bond identified by AIM is indicated by a broken line, which is labeled by the

TABLE III. Many-body analysis (kcal/mol) for the heterotrimers at MP2/aug-cc-pVTZ computational level.

Complex	Symmetry	Δ^3E	E_b
Tr1a	C_1	−0.05	−6.36
Tr1b	C_{2v}	0.01	−6.14
Tr1c	C_s	−0.25	−5.51
Tr2a	C_1	0.00	−7.38
Tr2b	C_1	−0.04	−7.20
Tr2c	C_1	−0.02	−7.06
Tr2d	C_s	0.07	−6.90
Tr2e	C_s	0.00	−6.80
Tr3a	C_1	0.00	−8.18
Tr3b	C_1	−0.24	−7.17
Tr3c	C_{2v}	−0.09	−7.12

interatomic distance (in black) and the density at the BCP (in red). Of the three minima for $(CO_2)_2$:H_2CO, Tr1A is the most stable. The carbonyl O is engaged in O··O chalcogen bonds with each of the two CO_2 molecules, contrary to its C··O bond in binary complexes 1A and 1B. Factoring in also the O··O bond between the two CO_2 molecules, Tr1a is bound by 6.36 kcal/mol and its stability rests in part on the O··O bond between the two CO_2 molecules. There is a second minimum Tr1b which lies only 0.2 kcal/mol higher in energy, with a different bonding scheme. This structure is quite similar to heterodimer 1A, with a CO_2 molecule on each side of H_2CO, bound by C··O and CH··O bonds. Tr1c is less stable, and relies on three separate C··O tetrel bonds, the strongest and shortest of these being the one involving the carbonyl O atom. The negative Δ^3E entry for Tr1c in Table III suggests it is favored by a small degree of positive cooperativity in this cyclic geometry, as compared to minimal cooperativity for the other two structures.

The five most stable minima for the $(CO_2)_2$:CH_3CHO heterotrimer are bunched within 0.5 kcal/mol of one another, all more strongly bound than $(CO_2)_2$:H_2CO. One of the two CO_2 molecules of Tr2a is arranged as in heterodimer 2A, containing both O··C and CH··O bonds. The auxiliary CO_2 molecule not only engages in an O··C bond with the carbonyl but also in an inter-CO_2 O··O bond. These O··O bonds are the sole source of the bonding in Tr2b, distinct from the four heterodimers 2A-2C which all depend upon a C··O bond. Indeed, such C··O bonding plays a prominent role in the next three $(CO_2)_2$:H_2CO 2:1 complexes, supplemented by O··O and CH··O bonds. Tr2e resembles a combination of the 2A and 2A′ heterodimers, with one CO_2 on either side of CH_3CHO, but supplemented by a long and weak inter-CO_2 O··O bond. The very small values of Δ^3E in Table III suggest minimal cooperativity in any of these heterotrimers.

The most stable Tr3a minimum of the $(CO_2)_2$:$(CH_3)_2CO$ system in Fig. 3 is separated from the next structure by a full kcal/mol. The carbonyl O··C bond to one CO_2 is augmented by O··O and CH··O bonds to the other. As judged by BCP densities, these three bonds are comparable in strength to one another. Even though Tr3b and Tr3c are very close in energy to one another, their bonding patterns are quite distinct: the former contains three O··C bonds, while Tr3c relies solely on O··O, as in heterodimer 3C. Due to the cyclic structure of Tr3b, there is a certain amount of positive cooperativity, with $\Delta^3E = -0.24$ kcal/mol. It is evident that cyclic structures reinforce the positive cooperativity.

TABLE IV. NBO analysis at ωB97XD/aug-cc-pVTZ computational level for the heterotrimers. Noncovalent interactions with an E(2) threshold greater than 0.3 kcal/mol.

Complex	Donor/acceptor	Type	E(2)
Tr1a	$H_2CO/CO_2(1)$	$O_{lp} \rightarrow \pi^*(CO_a)$	1.57
	$H_2CO/CO_2(2)$	$O_{lp} \rightarrow \pi^*(CO_d)$	0.70
	$CO_2(1)/CO_2(2)$	$O_{lp,b} \rightarrow \pi^*(CO_d)$	0.76
	$CO_2(2)/CO_2(1)$	$O_{lp,c} \rightarrow \pi^*(CO_a)$	0.70
Tr1b	H_2CO/CO_2	$O_{lp} \rightarrow \pi^*(CO_a)$	1.96[a]
Tr1c	$H_2CO/CO_2(1)$	$O_{lp} \rightarrow \pi^*(CO_a)$	0.89
	$CO_2(1)/CO_2(2)$	$O_{lp,b} \rightarrow \pi^*(CO_c)$	0.73
	$CO_2(2)/H_2CO$	$O_{lp,d} \rightarrow \pi^*(CO)$	1.10
Tr2a	$HCOCH_3/CO_2(1)$	$O_{lp} \rightarrow \pi^*(CO_a)$	1.38
	$HCOCH_3/CO_2(2)$	$O_{lp} \rightarrow \pi^*(CO_d)$	0.72
	$HCOCH_3/CO_2(2)$	$\pi(CO) \rightarrow \pi^*(CO_d)$	0.34
	$CO_2(1)/HCOCH_3$	$O_{lp,b} \rightarrow \sigma^*(CH)$	0.71
	$CO_2(1)/CO_2(2)$	$O_{lp,b} \rightarrow \pi^*(CO_d)$	0.67
	$CO_2(2)/CO_2(1)$	$O_{lp,c} \rightarrow \pi^*(CO_a)$	0.71
Tr2b	$HCOCH_3/CO_2(1)$	$O_{lp} \rightarrow \pi^*(CO_a)$	2.14
	$HCOCH_3/CO_2(2)$	$\pi(CO) \rightarrow \pi^*(CO_c)$	0.59
	$CO_2(2)/HCOCH_3$	$O_{lp,d} \rightarrow \pi^*(CO)$	1.47
	$CO_2(1)/CO_2(2)$	$O_{lp,b} \rightarrow \pi^*(CO_c)$	0.38
Tr2c	$HCOCH_3/CO_2(1)$	$O_{lp} \rightarrow \pi^*(CO_a)$	1.39
	$HCOCH_3/CO_2(1)$	$\pi(CO) \rightarrow \pi^*(CO_a)$	0.36
	$HCOCH_3/CO_2(2)$	$O_{lp} \rightarrow \pi^*(CO_c)$	0.80
	$CO_2(1)/CO_2(2)$	$\pi(CO_a) \rightarrow \pi^*(CO_c)$	0.42
Tr2d	$HCOCH_3/CO_2(1)$	$O_{lp} \rightarrow \pi^*(CO_a)$	1.45
	$HCOCH_3/CO_2(2)$	$O_{lp} \rightarrow \pi^*(CO)$	1.31
	$CO_2(1)/HCOCH_3$	$O_{lp,b} \rightarrow \sigma^*(CH)$	0.75
	$CO_2(1)/CO_2(2)$	$O_{lp,a} \rightarrow \pi^*(CO)$	0.38
Tr2e	$HCOCH_3/CO_2(1)$	$O_{lp} \rightarrow \pi^*(CO_a)$	2.42
	$HCOCH_3/CO_2(2)$	$O_{lp} \rightarrow \pi^*(CO_c)$	1.62
	$CO_2(2)/HCOCH_3$	$O_{lp,d} \rightarrow \sigma^*(CH)$	0.69
Tr3a	$(CH_3)_2CO/CO_2(1)$	$O_{lp} \rightarrow LV(C)$[b]	2.84
	$(CH_3)_2CO/CO_2(1)$	$O_{lp} \rightarrow \pi^*(CO_a)$	0.30
	$(CH_3)_2CO/CO_2(2)$	$\pi(CO) \rightarrow \pi^*(CO_c)$	0.74
	$CO_2(2)/(CH_3)_2CO$	$O_{lp,d} \rightarrow \pi^*(CO)$	1.46
	$CO_2(1)/CO_2(2)$	$O_{lp,b} \rightarrow \pi^*(CO_c)$	0.69
Tr3b	$(CH_3)_2CO/CO_2(1)$	$O_{lp} \rightarrow \pi^*(CO_a)$	1.36
	$CO_2(2)/(CH_3)_2CO$	$O_{lp,d} \rightarrow \pi^*(CO)$	1.01
	$CO_2(1)/CO_2(2)$	$O_{lp,b} \rightarrow \pi^*(CO_c)$	0.80
Tr3c	$(CH_3)_2CO/CO_2$	$\pi(CO) \rightarrow \pi^*(CO_a)$	0.73[a]
	$CO_2/(CH_3)_2CO$	$O_{lp,b} \rightarrow \pi^*(CO)$	1.69[a]

[a]Interactions which are duplicated due to the symmetry.
[b]LV refers to "lone vacant" orbital.

The NBO interpretation of the bonding patterns based on the E(2) values reported in Table IV are at times at odds with AIM data. Most notably, AIM predicts bond paths between atomic centers whereas it is usually an antibonding orbital between pairs of atoms which serves as the recipient of NBO

charge transfer. Taking Tr1a as an example, the strongest interaction of 1.57 kcal/mol arises from the NBO charge transfer from the carbonyl O to the π* antibond between C and O_a of CO_2. In contrast, AIM places this bond on O_b of the same CO_2 molecule. With respect to Tr1b, the AIM assessment of a pair of CH··O HBs fails to appear in the NBO framework, even using a fairly low threshold of 0.3 kcal/mol for E(2). As another example, the carbonyl O··O_b bond of Tr2b (Fig. 3) is interpreted by NBO instead as a charge transfer into the π*(CO_a) orbital. The inconsistencies of AIM predictions of bonds as compared to other methods are not a new observation, having been noted on previous occasions.[13,68,77–83] Some of these inconsistencies may be due in part to very nearly constant electron density in the relevant regions of weakly bonded complexes, i.e., molecular regions in which the density does not vary significantly manifest such discrepancies.

Some of these inconsistencies notwithstanding, there is a certain level of agreement between AIM and NBO pictures of the bonding in these ternary complexes. For example, all three AIM O··C bonds in Tr1c appear as $O_{lp} \rightarrow \pi^*(CO)$ charge transfers. As an added benefit, the NBO data can offer additional insights not available via AIM. The AIM carbonyl O··C bond of Tr2a is shown by NBO in Table IV to have three separate components. There is a charge transfer from the carbonyl O lone pairs into each of the π*(CO_a) and π*(CO_d) antibonding orbitals, which is supplemented by a $\pi(CO) \rightarrow \pi^*(CO_d)$ transfer. As another example, the carbonyl O··C bond in Tr2c is based on charge transfer into the π*(CO_a) orbital from both the O lone pairs and the π(CO) orbital, with the former making the larger contribution.

The addition of a third CO_2 molecule leads to the heterotetramers, with the three most stable of each type displayed in Fig. 4. As a distinguishing feature of all three solute systems, the most stable quaternary complex of each set relies principally on C··O tetrel bonds. For example, Te1a is stabilized by such bonds, combining the features of both heterodimers 1A and 1B (Table V). Te1b is slightly higher in energy and replaces some of the C··O bonds of Te1a by O··O interactions. All three types of noncovalent bonds are present in Te1c which is closely related to heterotrimer Tr1b. The three most stable heterotrimers incorporating CH_3CHO are of very similar energy. Like the H_2CO heterotetramers, the most stable Te2a complements its C··O bonds by a single CH··O. Te2b and Te2c substitute some of the C··O bonds by O··O. A similar pattern is evident in the $(CH_3)_2CO$ 3:1 complexes triad. As in the cases of heterodimers and trimers, the overall stability varies as $H_2CO < CH_3CHO < (CH_3)_2CO$. And again, there is only a small amount of cooperativity. $\Sigma\Delta^3E$ is less than 0.2 kcal/mol in all cases, despite the addition of four different triplets, and Δ^4E is essentially zero.

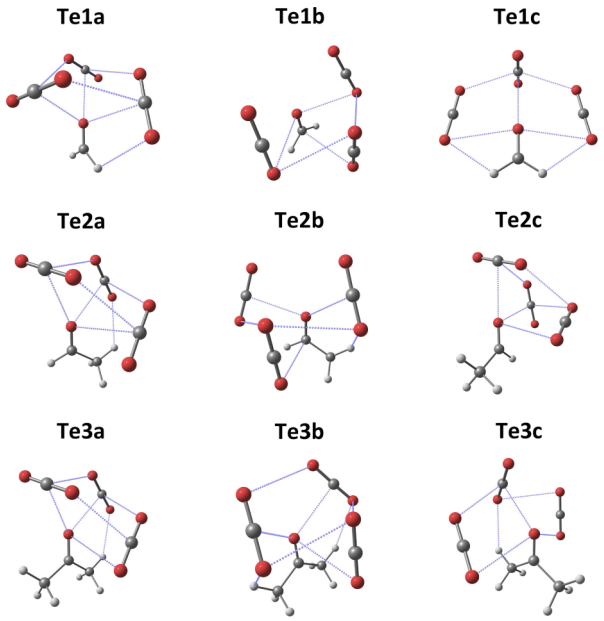

FIG. 4. Structures of minima on the potential energy surfaces of indicated heterotetramers at the MP2/aug-cc-pVDZ computational level. Broken lines are shown between atoms deemed by AIM to be connected by a bond critical point calculated via the MP2/aug-cc-pVTZ//MP2/aug-cc-pVDZ wavefunction.

TABLE V. Many-body analysis (kcal/mol) for the heterotrimers at MP2/aug-cc-pVTZ//MP2/aug-cc-pVDZ computational level.

Complex	Symmetry	$\Sigma\Delta^3E$	Δ^4E	E_b
Te1a	C_1	−0.12	0.01	−9.68
Te1b	C_s	−0.17	0.01	−9.33
Te1c	C_{2v}	0.12	0.02	−9.46
Te2a	C_1	−0.13	0.01	−10.91
Te2b	C_1	−0.14	0.01	−10.78
Te2c	C_1	−0.09	0.01	−10.72
Te3a	C_1	−0.09	0.00	−12.11
Te3b	C_1	−0.04	0.00	−11.94
Te3c	C_1	0.02	0.00	−11.26

There is the question as to whether the forces that determine the most stable heterodimers are transferred intact to larger aggregates. In the first place, the B structures from Fig. 2 in which the CO_2 C atom lies directly along the carbonyl C═O direction are limited only to the binary complexes. The A geometries, on the other hand, are a common feature of the ternary and quaternary complexes. For example, the combination of C··O and CH··O bonds, which is the distinguishing feature of A heterodimers, occurs in a wide range of different 2:1 and 3:1 complexes, even if not always the global minimum. The 3C geometry of CO_2:$(CH_3)_2CO$, which is the global minimum of this heterodimer, occurs as well in the global minimum of the 2:1 and 3:1 aggregates Tr3a and Te3a. From another perspective, cyclic heterotrimers and tetramers tend to be most common, but non-cyclic structures such as Tr1B and Tr3c, in which two of the molecules do not interact directly with one another, can be quite competitive energetically.

C··O bonds are commonly observed but are not mandatory. For example, the most stable $(CO_2)_2$:H_2CO heterotrimer Tr1a depends exclusively on O··O noncovalent bonds, as does the CO_2:$(CH_3)_2CO$, global minimum 3C. These C··O bonds rely on $O_{lp} \rightarrow \pi^*(CO)$ charge transfer, supplemented by $\pi(CO) \rightarrow \pi^*(CO)$. CH··O HBs occur in a number of aggregate geometries, but appear to be less common and weaker than C··O and O··O. Despite the occurrence of

multiple covalent bonds within these complexes, the degree of cooperativity is rather small.

SUMMARY AND DISCUSSION

The most stable 1:1 complexes are generally those of A type, which are characterized by an O··C bond to the C of CO_2, coupled with a CH··O HB. The latter bond is the decisive factor in the preference for A over B structures in which it is lacking. Both CH_3CHO and $(CH_3)_2CO$ contain a third C type of heterodimer on their potential energy surfaces with CO_2, characterized by an anti-parallel arrangement of the C═O bonds of the two molecules. The C structure of $(CH_3)_2CO$ represents the global minimum on its potential energy surface with CO_2. NBO analysis shows that the $O_{lp} \rightarrow \pi^*(CO)$ charge transfer from the carbonyl O is supplemented by a certain amount of transfer from π(CO) bonds in the C configurations. The binding energies of the various heterodimers vary between 2.4 and 3.5 kcal/mol (2.1 and 2.9 kcal/mol including counterpoise). The substitution of H atoms of H_2CO by methyl groups results in an incremental strengthening of the binding.

There are a host of different geometries adopted by the complexes of the carbonyl with 2 or 3 CO_2 molecules, with small energy differences separating them. The bonding features of the heterodimers are generally carried over to these larger heterotrimers and tetramers, although the linear C═O··C arrangement of the B binary complexes is largely absent. O··O chalcogen bonds, absent in the heterodimers, play a major role in many of these larger complexes. The degree of cooperativity in these oligomers is generally rather small, with a maximum positive cooperativity of only 0.25 kcal/mol.

While AIM and NBO pictures are consonant with one another in many cases, there are also a number of points of disagreement. Most notably, AIM noncovalent bonds are associated with particular atoms, one on each monomer. NBO, on the other hand, commonly identifies charge transfer into π* antibonds between pairs of atoms, and in some cases, the source of the charge is a π bonding orbital. There are also cases where AIM fails to indicate the presence of a noncovalent bond that is clearly suggested by NBO, and vice versa.

While Coulombic considerations certainly play an important role in the geometries adopted by these complexes, they are not dominant as there are other important issues as well. Many of the 1:1 complex geometries in Fig. 2 conform to expectations based on the electrostatic potentials of the monomers. The positive region of CO_2 generally lines up with the negative potential areas of the carbonyl solute molecules, and vice versa. For example, the positive potential on the equator of the CO_2 molecule overlaps with the negative region of the carbonyl O in the A and B heterodimer geometries, and likewise for the positive area around CH and the negative potential near the CO_2 O atom in the A structures. On the other hand, the π-hole above the carbonyl C atom of H_2CO and CH_3CHO does not appear to attract a CO_2 molecule, despite its fairly large magnitude. Indeed, it is only in 3C that a CO_2 O atom is located above the carbonyl C atom, but there is no π-hole in the $(CH_3)_2CO$ molecule. Even without a formal π-hole, however, it is evident that the anti-parallel alignment of the C═O bond in $(CH_3)_2CO$ and the C═O bond in CO_2 closest to it in 3C will result in an electrostatic attraction.

ACKNOWLEDGMENTS

This work has been supported by NSF-CHE-1026826 and by CTQ2012-35513-C02-02 (MINECO). Computer, storage, and other resources from the Division of Research Computing in the Office of Research and Graduate Studies at Utah State University and the CTI (CSIC) are gratefully acknowledged. Gratitude is also due to Professor Dr. Ibon Alkorta (IQM-CSIC) for the NBO analysis with the NBO6.0 program.

[1]D. G. Kaufman and C. M. Franz, *Biosphere 2000: Protecting Our Global Environment* (Kendall Hunt Publishing Co., 2000).
[2]T. R. Karl and K. E. Trenberth, Science **302**, 1719 (2003).
[3]J. M. DeSimone and W. Tumas, *Green Chemistry Using Liquid and Supercritical Carbon Dioxide* (Oxford University Press, 2003).
[4]C. Capello, U. Fischer, and K. Hungerbuhler, Green Chem. **9**, 927 (2007).
[5]V. K. Potluri, J. Xu, R. Enick, E. Beckman, and A. D. Hamilton, Org. Lett. **4**, 2333 (2002).
[6]F. Chang, H. Kim, B. Joo, K. Park, and H. Kim, J. Supercrit. Fluids **45**, 43 (2008).
[7]C. T. Estorach, M. Giménez-Pedrós, A. M. Masdeu-Bultó, A. D. Sayede, and E. Monflier, Eur. J. Inorg. Chem. **2008**, 2659.
[8]V. H. Dalvi, V. Srinivasan, and P. J. Rossky, J. Phys. Chem. C **114**, 15553 (2010).
[9]V. H. Dalvi, V. Srinivasan, and P. J. Rossky, J. Phys. Chem. C **114**, 15562 (2010).
[10]A. V. M. Nunes, A. P. C. Almeida, S. R. Marques, A. R. S. de Sousa, T. Casimiro, and C. M. M. Duarte, J. Supercrit. Fluids **54**, 357 (2010).
[11]I. Alkorta, F. Blanco, J. Elguero, J. A. Dobado, S. M. Ferrer, and I. Vidal, J. Phys. Chem. A **113**, 8387 (2009).
[12]C.-G. Liu, Mol. Phys. **111**, 259 (2012).
[13]L. M. Azofra and S. Scheiner, Phys. Chem. Chem. Phys. **16**, 5142 (2014).
[14]E. Orestes, C. M. Ronconi, and J. W. de Mesquita carneiro, Phys. Chem. Chem. Phys. **16**, 17213 (2014).
[15]P. Ramasami and T. A. Ford, Mol. Phys. **112**, 683 (2014).
[16]E. San-Fabián, F. Ingrosso, A. Lambert, M. I. Bernal-Uruchurtu, and M. F. Ruiz-López, Chem. Phys. Lett. **601**, 98 (2014).
[17]N. T. Trung, N. P. Hung, T. T. Hue, and M. T. Nguyen, Phys. Chem. Chem. Phys. **13**, 14033 (2011).
[18]M. Altarsha, F. Ingrosso, and M. F. Ruiz-López, ChemPhysChem **13**, 3397 (2012).
[19]M. Altarsha, V. Yeguas, F. Ingrosso, R. López, and M. F. Ruiz-López, J. Phys. Chem. B **117**, 3091 (2013).
[20]L. M. Azofra, M. Altarsha, M. F. Ruiz-López, and F. Ingrosso, Theor. Chem. Acc. **132**, 1326 (2013).
[21]L. Chen, F. Cao, and H. Sun, Int. J. Quantum Chem. **113**, 2261 (2013).
[22]N. T. Trung and M. T. Nguyen, Chem. Phys. Lett. **581**, 10 (2013).
[23]C. L. Christenholz, R. E. Dorris, R. A. Peebles, and S. A. Peebles, J. Phys. Chem. A **118**, 8765 (2014).
[24]H. Q. Dai, N. N. Tri, N. T. T. Trang, and N. T. Trung, RSC Adv. **4**, 13901 (2014).
[25]M. G. Frysali, E. Klontzas, and G. E. Froudakis, ChemPhysChem **15**, 905 (2014).
[26]M. Hidalgo, R. Rivelino, and S. Canuto, J. Chem. Theory Comput. **10**, 1554 (2014).
[27]H.-C. Li, J.-D. Chai, and M.-K. Tsai, Int. J. Quantum Chem. **114**, 805 (2014).
[28]V. T. Phuong, N. T. T. Trang, V. Vo, and N. T. Trung, Chem. Phys. Lett. **598**, 75 (2014).
[29]R. E. Rosenfield, R. Parthasarathy, and J. D. Dunitz, J. Am. Chem. Soc. **99**, 4860 (1977).
[30]F. T. Burling and B. M. Goldstein, J. Am. Chem. Soc. **114**, 2313 (1992).
[31]R. M. Minyaev and V. I. Minkin, Can. J. Chem. **76**, 776 (1998).
[32]M. Iwaoka, S. Takemoto, and S. Tomoda, J. Am. Chem. Soc. **124**, 10613 (2002).

[33]P. Sanz, M. Yáñez, and O. Mó, J. Phys. Chem. A **106**, 4661 (2002).
[34]P. Sanz, M. Yáñez, and O. Mó, New J. Chem. **26**, 1747 (2002).
[35]P. Sanz, M. Yáñez, and O. Mó, Chem. - Eur. J. **8**, 3999 (2002).
[36]D. B. Werz, R. Gleiter, and F. Rominger, J. Am. Chem. Soc. **124**, 10638 (2002).
[37]P. Sanz, O. Mo, and M. Yanez, Phys. Chem. Chem. Phys. **5**, 2942 (2003).
[38]C. Bleiholder, D. B. Werz, H. Köppel, and R. Gleiter, J. Am. Chem. Soc. **128**, 2666 (2006).
[39]G. Sánchez-Sanz, I. Alkorta, and J. Elguero, Mol. Phys. **109**, 2543 (2011).
[40]M. Jabłoński, J. Phys. Chem. A **116**, 3753 (2012).
[41]G. Sánchez-Sanz, C. Trujillo, I. Alkorta, and J. Elguero, ChemPhysChem **13**, 496 (2012).
[42]A. Bauzá, I. Alkorta, A. Frontera, and J. Elguero, J. Chem. Theory Comput. **9**, 5201 (2013).
[43]U. Adhikari and S. Scheiner, J. Phys. Chem. A **118**, 3183 (2014).
[44]L. M. Azofra and S. Scheiner, J. Phys. Chem. A **118**, 3835 (2014).
[45]L. M. Azofra, I. Alkorta, and S. Scheiner, J. Chem. Phys. **140**, 244311 (2014).
[46]L. M. Azofra, I. Alkorta, and S. Scheiner, Phys. Chem. Chem. Phys. **16**, 18974 (2014).
[47]L. M. Azofra, I. Alkorta, and S. Scheiner, Theor. Chem. Acc. **133**, 1586 (2014).
[48]V. d. P. N. Nziko and S. Scheiner, J. Phys. Chem. A **118**, 10849 (2014).
[49]I. Alkorta, I. Rozas, and J. Elguero, J. Phys. Chem. A **105**, 743 (2001).
[50]A. Bauzá, T. J. Mooibroek, and A. Frontera, Angew. Chem., Int. Ed. **52**, 12317 (2013).
[51]S. J. Grabowski, Phys. Chem. Chem. Phys. **16**, 1824 (2014).
[52]M. R. Nelson and R. F. Borkman, J. Phys. Chem. A **102**, 7860 (1998).
[53]M. A. Blatchford, P. Raveendran, and S. L. Wallen, J. Phys. Chem. A **107**, 10311 (2003).
[54]R. Rivelino, J. Phys. Chem. A **112**, 161 (2008).
[55]K. H. Kim and Y. Kim, J. Phys. Chem. A **112**, 1596 (2008).
[56]C. Møller and M. S. Plesset, Phys. Rev. **46**, 618 (1934).
[57]T. H. Dunning, J. Chem. Phys. **90**, 1007 (1989).
[58]S. F. Boys and F. Bernardi, Mol. Phys. **19**, 553 (1970).
[59]M. J. Frisch, G. W. Trucks, H. B. Schlegel, G. E. Scuseria, M. A. Robb, J. R. Cheeseman, G. Scalmani, V. Barone, B. Mennucci, G. A. Petersson, H. Nakatsuji, M. Caricato, X. Li, H. P. Hratchian, A. F. Izmaylov, J. Bloino, G. Zheng, J. L. Sonnenberg, M. Hada, M. Ehara, K. Toyota, R. Fukuda, J. Hasegawa, M. Ishida, T. Nakajima, Y. Honda, O. Kitao, H. Nakai, T. Vreven, J. A. Montgomery, J. E. Peralta, F. Ogliaro, M. Bearpark, J. J. Heyd, E. Brothers, K. N. Kudin, V. N. Staroverov, R. Kobayashi, J. Normand, K. Raghavachari, A. Rendell, J. C. Burant, S. S. Iyengar, J. Tomasi, M. Cossi, N. Rega, N. J. Millam, M. Klene, J. E. Knox, J. B. Cross, V. Bakken, C. Adamo, J. Jaramillo, R. Gomperts, R. E. Stratmann, O. Yazyev, A. J. Austin, R. Cammi, C. Pomelli, J. W. Ochterski, R. L. Martin, K. Morokuma, V. G. Zakrzewski, G. A. Voth, P. Salvador, J. J. Dannenberg, S. Dapprich, A. D. Daniels, Ö. Farkas, J. B. Foresman, J. V. Ortiz, J. Cioslowski, and D. J. Fox, GAUSSIAN09, Revision D.01, Gaussian, Inc., Wallingford CT, 2009.
[60]H.-J. Werner, P. J. Knowles, F. R. Manby, M. Schütz, P. Celani, G. Knizia, T. Korona, R. Lindh, A. Mitrushenkov, G. Rauhut, T. B. Adler, R. D. Amos, A. Bernhardsson, A. Berning, D. L. Cooper, M. J. O. Deegan, A. J. Dobbyn, F. Eckert, E. Goll, C. Hampel, A. Hesselmann, G. Hetzer, T. Hrenar, G. Jansen, C. Köppl, Y. Liu, A. W. Lloyd, R. A. Mata, A. J. May, S. J. McNicholas, W. Meyer, M. E. Mura, A. Nicklaß, P. Palmieri, K. Pflüger, R. Pitzer, M. Reiher, T. Shiozaki, H. Stoll, A. J. Stone, R. Tarroni, T. Thorsteinsson, M. Wang, and A. Wolf, MOLPRO, version 2012.1, a package of *ab initio* programs, 2012, see http://www.molpro.net.
[61]S. S. Xantheas and T. H. Dunning, J. Chem. Phys. **99**, 8774 (1993).
[62]S. S. Xantheas, J. Chem. Phys. **100**, 7523 (1994).
[63]F. Weinhold and C. R. Landis, *Valency and Bonding. A Natural Bond Orbital Donor-Aceptor Perspective* (Cambridge Press, Cambridge, UK, 2005).
[64]J.-D. Chai and M. Head-Gordon, Phys. Chem. Chem. Phys. **10**, 6615 (2008).
[65]E. D. Glendening, J. K. Badenhoop, A. E. Reed, J. E. Carpenter, J. A. Bohmann, C. M. Morales, C. R. Landis, and F. Weinhold, *NBO 6.0* (Theoretical Chemistry Institute, University of Wisconsin, Madison, USA, 2013).
[66]R. F. W. Bader, *Atoms in Molecules: A Quantum Theory* (Clarendon Press, Oxford, UK, 1990).
[67]T. A. Keith, *AIMAll, version 13.11.04* (TK Gristmill Software, Overland Park KS, USA, 2013).
[68]E. R. Johnson, S. Keinan, P. Mori-Sánchez, J. Contreras-García, A. J. Cohen, and W. Yang, J. Am. Chem. Soc. **132**, 6498 (2010).
[69]J. S. Murray and P. Politzer, WIREs Comput. Mol. Sci. **1**, 153 (2011).
[70]F. Bulat, A. Toro-Labbé, T. Brinck, J. Murray, and P. Politzer, J. Mol. Model. **16**, 1679 (2010).
[71]J. P. Perdew, K. Burke, and M. Ernzerhof, Phys. Rev. Lett. **77**, 3865 (1996).
[72]G. Chałasiński and M. M. Szczęśniak, Chem. Rev. **100**, 4227 (2000).
[73]L.-S. Wang, J. E. Reutt, Y. T. Lee, and D. A. Shirley, J. Electron Spectrosc. Relat. Phenom. **47**, 167 (1988).
[74]J. C. Traeger, Int. J. Mass Spectrom. Ion Processes **66**, 271 (1985).
[75]M. A. Blatchford, P. Raveendran, and S. L. Wallen, J. Am. Chem. Soc. **124**, 14818 (2002).
[76]A. P. Sergeeva, B. B. Averkiev, H.-J. Zhai, A. I. Boldyrev, and L.-S. Wang, J. Chem. Phys. **134**, 224304 (2011).
[77]M. Jabłoński and M. Palusiak, Chem. Phys. **415**, 207 (2013).
[78]I. Alkorta, G. Sánchez-Sanz, J. Elguero, and J. E. Del Bene, J. Phys. Chem. A **118**, 1527 (2014).
[79]L. M. Azofra and S. Scheiner, J. Chem. Phys. **140**, 034302 (2014).
[80]R. A. Cormanich, R. Rittner, D. O'Hagan, and M. Bühl, J. Phys. Chem. A **118**, 7901 (2014).
[81]C. Foroutan-Nejad, S. Shahbazian, and R. Marek, Chem. - Eur. J. **20**, 10140 (2014).
[82]P. R. Varadwaj, A. Varadwaj, and B.-Y. Jin, Phys. Chem. Chem. Phys. **16**, 17238 (2014).
[83]F. Weinhold, P. v. R. Schleyer, and W. C. McKee, J. Comput. Chem. **35**, 1499 (2014).
[84]See supplementary material at http://dx.doi.org/10.1063/1.4905899 for Fig. S1 and Table S1. There, NCI and DFT-SAPT analyses can be seen.